Effects of the Au(I)–Au(I) Closed-Shell Attraction on the Electronic and Phosphorescent Properties in a Series of Coordination Compounds: A Theoretical Study

JESÚS MUÑIZ,[1] ENRIQUE SANSORES,[2] J. A. REYES-NAVA,[1] V.-H. RAMOS-SANCHEZ,[1] ALFREDO OLEA[1]

[1]*Cuerpo Académico de Energía y Sustentabilidad, Universidad Politécnica de Chiapas, Calle Eduardo J. Selvas S/N, Col. Magisterial, Tuxtla Gutiérrez, Chiapas, México C.P. 29010*

[2]*Instituto de Investigaciones en Materiales, Universidad Nacional Autónoma de México. Apartado Postal 70-360, México DF 04510, México*

Received 26 September 2010; accepted 20 October 2010
Published online 1 February 2011 in Wiley Online Library (wileyonlinelibrary.com).
DOI 10.1002/qua.22986

ABSTRACT: The Au(I)–Au(I) closed-shell or aurophilic attraction has been the subject of interest in the experimental and theoretical chemistry fields, due to the intriguing properties associated to it. The presence of phosphorescence in "aurophilic" compounds has been addressed to a wide range of applications, but it has not yet been fully understood. A theoretical study on the electronic and phosphorescent properties of the following series of dinuclear gold complexes has been performed: [Au_2(dmpm)(i-mnt)] (**1**), [Au_2(μ-Me-TU) (μ-dppm)] (**2**), and [Au_2(μ-G)(μ-dmpe)] (**3**). Full geometry optimizations at the second-order Møller–Plesset perturbation theory (MP2) were carried out for each of the species. These calculations made evident that, at the ground-state geometry, the Au(I) cations allocated at the center of the ring show a short Au–Au distance below the sum of the van der Waals radii, at the range of the aurophilic attraction. An intermolecular Au(I)–Au(I) closed-shell attraction for a pair of the systems under study is found. This attraction is comparable to that of the hydrogen bonds. The phosphorescent properties experimentally observed for this series were also characterized through ab initio techniques. The obtained results allow to fit reasonably

Correspondence to: J. Muñiz; e-mail: jmuniz@upchiapas.edu.mx

Contract grant sponsors: IMPULSA, PUNTA.
Contract grant number: PAPIIT-IN107807.
Contract grant sponsor: PROMEP-SEP.
Contract grant numbers: UPCHS-PTC-039, UPCHS-PTC-018.

the excitation energies with the experimental data and to identify a correlation between the strength of the Au(I)–Au(I) interaction and the phosphorescent behavior. © 2011 Wiley Periodicals, Inc. Int J Quantum Chem 111: 4378–4388, 2011

Key words: aurophilic attraction; phosphorescence; ab initio calculations; excited states

1. Introduction

Au(I) compounds have a wide field of applications, ranging from sensor design and electronic devices [1–3], biosensors [4], photocatalysts [5] and nanowires [6] to gold-based drugs used on antiarthritic treatment and chemotherapy [7–10]. For instance, auranofin is a drug used in rheumatoid arthritis treatment. Auranofin is a neutral Au(I) thiolate compound, where it is believed that the interaction between the protein and the Au(I) cation exerts the therapeutic action [9, 10]. It has recently been found that the mixed-metal compounds with closed-shell attractions [11] have a potential use in catalytic activity. Some of those compounds are luminescent under certain conditions. Above all, it has been reported that the dinuclear Au(I) [12] and bimetallic Au(I)–Ag(I) [11] species present an emission band after the exposure to UV radiation. In other systems, the light emission emerges after the compound has undergone direct contact [13, 14] with a solvent (solvoluminescence) or a gas (vapochromism) [15]. There are other remarkable cases in which the luminescence is activated after mechanical compression (luminescence tribochromism) [16].

The luminescent behavior appears to be associated to the closed-shell interaction termed aurophilic attraction. In particular, some Au(I) coordination complexes with short Au(I)–Au(I) contacts exhibit this interaction. Several phenomena are associated with aurophilicity, and striking properties are addressed to it. The aurophilic attraction is a van der Waals-type interaction, comparable in energy to the weakest covalent bonding and the strongest hydrogen bonds [17]. It is characterized by Au–Au contacts below the sum of the van der Waals radii for gold (~360 pm). It is known that the mechanism behind this interaction is mainly ruled by dispersion [18] and strengthened by relativistic effects [19].

It has been stated that the luminescence may be related to the aurophilic attraction [20]; i.e., it seems that the aurophilic interactions are connected to the radiation emitted by the complex. Indeed, when the Au(I)–Au(I) attraction is absent, the luminescence is absent as well. Nevertheless, this behavior is exactly the opposite in other systems [20].

The systems under study are the following ring complexes: $[Au_2(dmpm)(i\text{-}mnt)]$ (**1**), $[Au_2(\mu\text{-}MeTU)(\mu\text{-}dppm)]$ (**2**), and $[Au_2(\mu\text{-}G)(\mu\text{-}dmpe)]$ (**3**). Complex **1** has been synthesized by Tang et al. [21]. It is an eight-member ring with a thiolate ligand [see Fig. 1(a)]. It presents an Au(I)–Au(I) closed-shell attraction of the aurophilic type at the intramolecular and intermolecular levels.

The dmpm ligand corresponds to the diphosphine group, whereas i-mnt = $S_2C_2(CN)_2^{2-}$ is the dithiolate group. The Au(I) cations are bridged by both ligands. Compound **1** has an emission band at 558 nm at room temperature in acetonitrile solution and also at 77 K in solid-state phase. This complex has been chosen for study because it is a representative species of the Tang's series, and the number of electrons associated to it is computationally manageable. Furthermore, the electronic structure information combined with the experimental data may aid in the design of Au(I) compounds for the treatment of arthritis and tumors, among other applications.

Compound **2** [see Fig. 1(b)] has been recently synthesized by Lee and Eisenberg [16], with strong aurophilic contacts at the solid-state phase, expanding in a helicoidal arrangement formed by the Au(I)–Au(I) intramolecular (~288 pm) and intermolecular (~333 pm) interactions. This system presents a unique property among the metallic compounds called luminescence tribochromism: It is assigned to the emission of light after the compound has undergone a mechanical compression. The phosphorescent behavior may be turned off via acidity control. The absorption band is located at 375 nm, while there are several emission bands with a maximum centered at 483 nm.

An interesting issue to be explored relating the closed-shell attractions is the search of new transition metal complexes containing nucleobases derivatives [21]. This is examined to understand

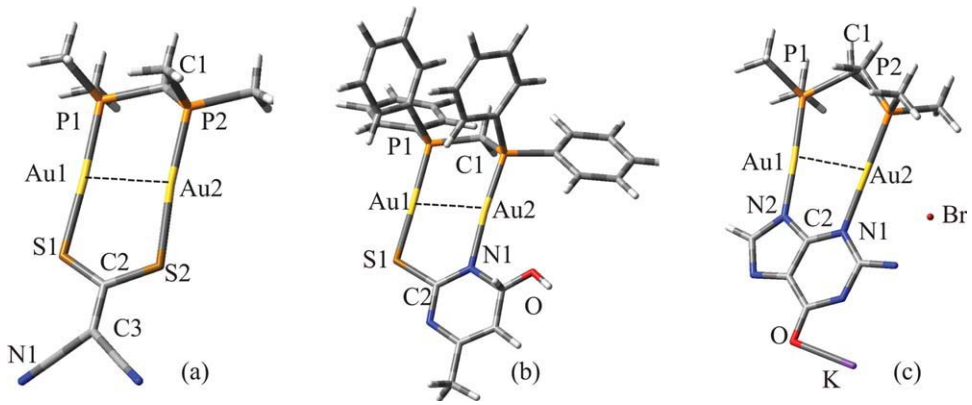

FIGURE 1. Complexes (a) [Au_2(dmpm)(i-mnt)] (**1**), (b) [Au_2(μ-Me-TU) (μ-dppm)] (**2**), and (c) [Au_2(μ-G)(μ-dmpe)] (**3**) at the MP2 ground-state geometry. [Color figure can be viewed in the online issue, which is available at wileyonlinelibrary.com.]

the acid metal–nucleic interactions to get information about several biological phenomena and to stimulate the quest of new biologically active metallodrugs. As a matter of fact, the Au(I)–phosphine metallodrugs have been successfully used as antiarthritic and antitumoral agents. However, despite the existence of several metallic complexes structurally characterized, only four systems in which the guanine (H_2G) molecule is coordinated to metallic ions have been reported [21].

Complex **3** has been chosen to complete this study because of further properties associated to the observed aurophilic attraction. This complex has been recently synthesized by Colacio et al. [22], and it is characterized by a metal–guanine bonding. The understanding of the mechanism governing such bonding and its possible relation with the phosphorescent behavior is of high relevance. This system is a nine-member ring with K^+ and Br^- ions, and water molecules are involved in hydrogen bonding or weak K···O interactions.

Au(I) atoms in Figure 1(c) are bridged by the diphosphine ligand and the guaninate anion. The experimental Au(I)—Au(I) bond length is 303 pm. This is the first example where two N atoms are bridged to guanine, and intermolecular contacts are absent. The system is phosphorescent at room temperature and at 77 K in the solid-state phase with an absorption band centered at 385 nm and two emission bands located at 452 and 449 nm.

Simplified ring molecular systems with aurophilic attractions, where extended ligands are substituted by hydrogen atoms, have been previously studied [23, 24]. This simplification appears to be useful, but lacks of generality. There is a limited number of theoretical studies on nonsimplified systems with metallophilic interactions. In the systems [$AuS_2PPh(OCH_2CH{=}CH_2)]_2$ [17], [Au_2(carb)$_2$Ag(μ-3,5-Ph_2pz)], and [Au(im)CH_3(pz)Ag_2(μ-3,5-H_2pz)$_2$] [25] studied by Muñiz et al., the metallophilic attractions were strengthened in the excited state, stimulating the increase of phosphorescence, but a clear correlation between the aurophilic attraction in dinuclear Au(I) systems and the phosphorescent behavior has not been established. The aim of this work is to contribute to the understanding of the aurophilic attraction and the relation with phosphorescence properties.

2. Computational Methods

Geometry optimizations were performed with second-order Møller–Plesset perturbation theory, the MP2 [26] computational method, which explicitly accounts for dispersion effects, important in the description of aurophilic interactions. A treatment on spin-orbit effects is not included here, because it is known that they are not important to Au(I) systems [27, 28]. The Stuttgart small-core pseudo-relativistic effective core potential [29] with 19 valence electrons was used for gold. The effective core potential was used with the valence triple-f plus one polarization type; that is, the basis set TZVP, which is an optimized contracted Gaussian basis set for Au, was calculated [30] with the same methodology than that of the basis computed by Schäfer et al. [31]. Two

additional f-type polarization functions calculated by Pyykkö et al. [32] were augmented to the basis set ($\alpha_f = 0.2, 1.19$). The first function is a diffuse f orbital necessary for the intermolecular interaction, whereas the second is a polarization function, important for describing the covalent bonding, involving the Au d^{10} shell. For the non-Au atoms (C, N, O, P, S, Br, K, and H), the TZVP basis set was used [31, 33]. Basis Set Superposition Error calculations were performed in accordance to the Counterpoise (CP) methodology developed by Boys and Bernardi [34] at the Resolution of Identity MP2 level (RI-MP2) [35–38]. The interaction energy was calculated according to Eq. (1):

$$V(R) = E_{AB}^{AB}(R) - E_{A}^{AB}(R) - E_{B}^{AB}(R), \qquad (1)$$

where the lower index refers to the system treated, whereas the upper index refers to the basis set used. The excited-state computations were performed using the CIS computational methodology [39]. Orbital populations were obtained according to the NBO method [40]. The RI-MP2 calculations were performed with the Quantum Chemistry software Turbomole 5.9 [41, 42], whereas the rest of the computations were carried out using the Gaussian03 code [43].

3. Results and Discussion

3.1. STRUCTURAL DESCRIPTION

A full geometry optimization was performed at the MP2 level to study the aurophilic attraction observed in complex **1**; the main structural parameters are shown in Table I, and the molecular geometry is depicted in Figure 1(a). The optimized geometry does not present point group symmetry; the Au—Au bond length is 289 pm [21] in the solid-state phase, whereas the calculated bond length in this work is 300 pm. The latter corresponds to a weak interaction of the aurophilic type, because the calculated bond length is below the sum of the van der Waals radii (360 pm).

The optimized Au—P bond lengths (241 pm) appear to be slightly longer than those found in the experiment (see Table I). Such discrepancy on the optimized parameters from those found experimentally may be attributed to the fact that compound **1** was characterized in the solid-state phase, whereas the optimization was performed at the gas phase. Minor deviations are also found

TABLE I
MP2 bond lengths and angles of complex 1.

	MP2	Experiment
Bond (pm)		
Au1—Au2	300	289
Au1—P1	228	225
Au1—S1	233	232
S1—C2	179	172
P1—C1	191	189
C2—C3	137	146
Bond angle (°)		
P2—Au2—S2	176.7	175.4
P1—C1—P2	112.4	112.0
S1—C2—S2	120.5	125.9

on the Au–S and S–C bond lengths; the P – C bonds are adequately reproduced, presenting only deviations of about 2 pm. The optimized P—Au—S bond angles around the ring are collinear, in accordance with experimental data, which suggests that the compound exhibits a quasi-planar ring structure, where the Au atoms are located at the center [see Fig. 1(a)].

The dinuclear Au(I) complex (**2**) presents a thiouracilate as a ligand and exhibits a luminescent phenomenon called luminescence tribochromism: Light emission arises when a mechanical compression is exerted on the surface at the solid-state phase. Complex **2** is an eight-member ring with the Au atoms lying at the center; the thiouracilate ligand is attached at the lower side of the complex [see Fig. 1(b)], whereas the P atoms are bonded to the Au(I) cations by the dppm = bis(diphenylphosphine)methane ligand. Intra- and intermolecular aurophilic attractions have been reported according to Lee and Eisenberg [16]; the intramolecular Au—Au bond length is 286 pm at the solid state, whereas the intermolecular Au—Au bond length is 333 pm.

The MP2 ground-state geometry is presented in Figure 1(b), and the main structural parameters are shown in Table II. The optimized Au—Au bond length is 298 pm, corresponding to a value below the van der Waals radii (~360 pm). This value differs from experimental data by 12 pm, indicating a strong aurophilic attraction. The rest of the structural parameters are in reasonable agreement with those found at the solid-state phase. Complex **2** is also a quasi-planar ring with a slight deviation located on the thiouracilate; the S1—Au2—P2 bond angle is 175°, consistent with that found experimentally at 176°; the N1—Au1—P1 bond angle of 173.0° is also in agreement with 178.6° found through experiments.

TABLE II
MP2 bond lengths and angles of complex 2.

	MP2	Experiment
Bond (pm)		
Au1—Au2	298	286
Au2—N1	205	209
Au1—P1	230	224
Au1—S1	232	232
P1—C1	189	183
N1—C2	137	135
Bond angle (°)		
P1—Au1—S1	176.7	175.4
P1—C1—P2	115.7	115.2
N1—C2—S1	121.6	122.3

On the other hand, K^+ and O^- ions, located about the (μ-dmpe) ligand, as well as the water molecules within the complex [[Au_2(μ-G)(μ-dmpe)](KBr)0.75 $2H_2O$] have been omitted for its study because it is known that they have no influence on its luminescent properties [22]. Hence, the resulting system [Au_2(μ-G)(μ-dmpe)] (complex **3**) was fully optimized at the MP2 level. The ground-state geometry is shown in Figure 1(c), and the main structural parameters are reported in Table III: The Au—Au bond length is slightly longer than that observed in the experiment. When the calculation is performed with the Br^- ion, which is close to the Au atoms, the Au–Au distance is shortened, and an excellent agreement is achieved (see Table III). This is a clear indication that the Br^- ion induces the aurophilic attraction for this system.

3.2. ELECTRONIC STRUCTURE

To study the electronic nature of the Au–Au interaction in complex **1**, an NBO calculation was performed, and the results are presented in Table IV. The Au atoms are positively charged, whereas the P and S ligands show positive and negative charge, respectively, which means that the electronic charge is transferred to the S and C atoms on the dmpm ligand. The small amount of charge on the Au atoms yields the breaking of the $5d^{10}$ $6s^0$ closed-shell structure and the rising of the new electronic configurations $5d^{9.82}$ $6s^{0.71}$ $7p^{0.02}$ and $5d^{9.82}$ $6s^{0.69}$ $7p^{0.02}$ for the Au1 and Au2 atoms, respectively (see Fig. 1). Because the electrons at the S atoms are shared with the Au atoms, the 6s and 7p empty orbitals are partially populated, driving the observed weak Au(I)–Au(I) attraction, i.e., the aurophilic bonding is also produced by a hybridization among the formally filled 5d shell and the empty 6s and 7p shells of the Au(I) atoms. The Au(I) atomic orbitals are asymmetrically filled because of the lack of point group symmetry on the molecule.

TABLE III
MP2 bond lengths and angles of complex 3.

	MP2	MP2 (anion)[a]	Experiment
Bond (pm)			
Au1—Au2	311	309	303
Au2—N1	212	206	212
Au1—P1	239	227	226
K—O	273	262	282
Bond angle (°)			
P1—Au1—N2	177.4	176.5	174.0
N1—C2—N2	128.8	127.6	133.3
P1—C1—P2	107.3	110.7	113.1

[a] Calculation performed with the Br anion.

TABLE IV
Selected NBO atomic charges of complex 1.

Atom	MP2
Au1	0.338
Au2	0.348
P1	0.832
S1	−0.314
C1	−1.067
N1	−0.268
Dipole (D)	0.0

The calculation of the Wiberg bond order [44] between the Au atoms was also computed with a 0.0887 value, which certainly indicates the presence of a weak interaction between the cations.

Compound **1** shows an intermolecular aurophilic attraction among adjacent Au(I) atoms on each of the molecules, forming the polymeric structure observed in the solid state [see Fig. 2(a)]. A CP interaction energy calculation [34] was performed at the equilibrium geometry observed experimentally. The computation was performed in a dimer [see Fig. 2(a)], in accordance with Eq. (1) and using the RI-MP2 method; a value of 13.3 kcal/mol was obtained at an intermolecular Au(I)–Au(I) distance of 320 pm. This interaction energy is in agreement with the well-known range of the aurophilic energy (10–15 kcal/mol) [17]. However, the SCF energy for this configuration overestimates by about 10 kcal/mol the aurophilic energy range, which confirms that the

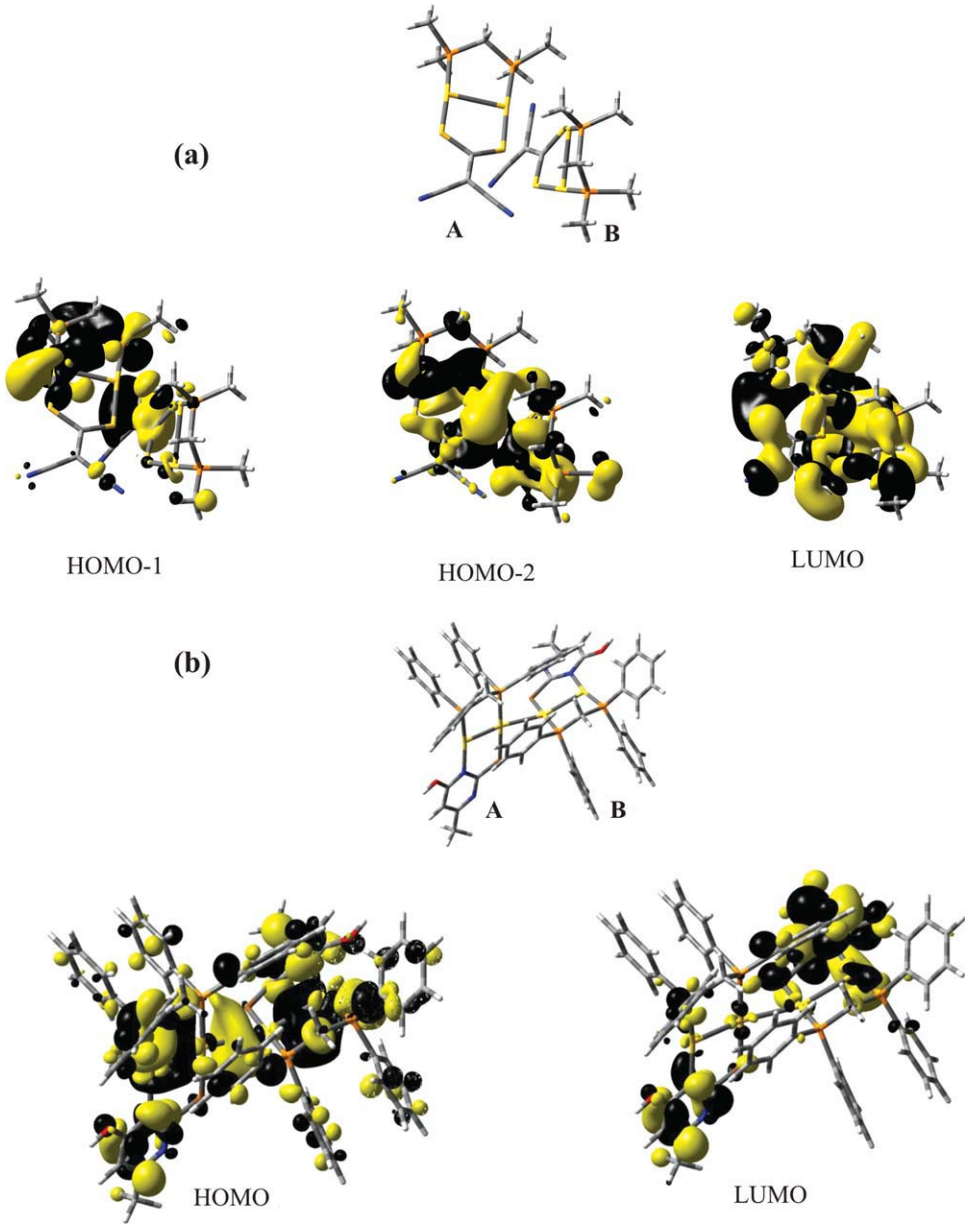

FIGURE 2. (a) Molecular geometry of $[Au_2(dmpm)(i\text{-}mnt)]_2$ and its corresponding frontier molecular orbitals. (b) Molecular geometry of $[Au_2(\mu\text{-Me-TU})\ (\mu\text{-dppm})]_2$ and its corresponding frontier molecular orbitals. [Color figure can be viewed in the online issue, which is available at wileyonlinelibrary.com.]

dispersive contribution is crucial in the description of the Au(I)–Au(I) closed-shell attraction.

The bonding character of the intermolecular interaction may also be interpreted from the spatial representation of the frontier molecular orbitals (MOs) at the equilibrium geometry, as it is depicted by the SCF isosurfaces [Fig. 2(a)]. Lower energy MOs also play an important role in the interaction. The HOMO-1 and HOMO-2 are mainly localized in the region between the molecules; they are formed by Au d_z^2 orbitals allocated at the Au atoms and p orbitals allocated at the P atoms. The aforesaid indicates that a dp-like hybridization may also be responsible for the aurophilic attraction seen in experiment. The LUMO presents an antibonding configuration, and it is located at the center of the rings, as shown in Figure 2(a). The LUMO is composed of

TABLE V
Selected NBO atomic charges of complex 2.

Atom	MP2
Au1	0.398
Au2	0.271
N1	−0.737
C2	0.329
S1	−0.315
P1	0.865
Dipole (D)	0.0

the Au 6s orbitals and a mixture of sp orbitals coming from the P atoms.

According to the NBO charges (see Table V), the Au atoms and P ligands in compound **2** possess an excess positive charge. The S and N atoms bonded to the Au atoms are negatively charged, while the thiouracilate ligand presents a total charge of −0.812, indicating that the Au atoms and the ligand share electrons. The dppm ligand has a negative charge excess of −1.041.

The electronic configuration of the Au1 atom [see Fig. 1(b)] is the following: $5d^{9.70}6s^{0.86}6p^{0.01}7p^{0.02}$; such result corroborates that the Au(I) $5d^{10}$ closed-shell electronic structure is lost and an open-shell electronic structure is formed instead. An analogous behavior is found on the Au2 atom, with electronic configuration $5d^{9.76}6s^{0.92}6p^{0.01}7p^{0.03}$. This hybridization, analogous to that observed in complex **1**, may also be interpreted as one of the mechanisms behind the shrinking of the Au—Au bond length, originating the aurophilic attraction observed experimentally. In addition, the Wiberg bond order between the Au(I) atoms also computed at the MP2 level of theory returned a value of 0.0752, characteristic of the weak interaction assigned to the aurophilic attraction [45].

WBO calculations were performed on complex **2** to compare the order of magnitude of the Au(I) closed-shell interaction with respect to that observed in small-sized (Au_2) and large-sized systems (Au_{20}). For the Au_2 system, a value of 0.9378 was obtained, equivalent to the covalent bonding where two electrons are shared. The electronic structure of the Au_{20} cluster approaches that of gold in the bulk phase, where the metallic character of the bonding is expected. The WBO for the Au_{20} is 0.1504, calculated for the closest neighbors within the system. As a consequence, the order of magnitude of the aurophilic attraction observed in complex **1** and **2** is much weaker than the typical covalent and metallic bonding.

The intermolecular aurophilic interaction was also studied from a CP-corrected RI-MP2 calculation at the experimental equilibrium structure with an intermolecular Au(I)–Au(I) bonding distance of 292 pm. A value of 12.8 kcal/mol was obtained (this energy is overestimated by 4.2 kcal/mol at the SCF level). As it was found in complex **1**, this behavior may also be due to a strong aurophilic attraction.

According to the frontier MO isosurfaces, the $[Au_2(\mu\text{-Me-TU})\ (\mu\text{-dppm})]_2$ (**2**) HOMO exhibits an important contribution at the intermediate volume between the monomers [see Fig. 2(b)]. This contribution is mainly formed by the Au6s orbitals, and the excess charge located at this region strengthens the bonding. This behavior may be interpreted as one of the mechanisms giving rise to the aurophilic attraction found in experiment. Furthermore, the intramolecular aurophilic attraction is also strengthened by the excess charge coming from the bonding of Au6s orbitals allocated at the center of the ring of each monomer [see Fig. 2(b)].

With regard to the electronic configuration of the Au1 and Au2 atoms in complex (**3**), these present $5d^{9.71}6s^{0.84}6p^{0.03}6d^{0.01}$ and $5d^{9.70}6s^{0.88}6p^{0.02}6d^{0.01}$, respectively. It is observed that, as the other systems presented in this work, the 6s and 6p orbitals are partially filled, whereas the 5d shell is broken. No intermolecular interactions are found at this level of theory for compound (**3**), in agreement with the experimental results reported by Colacio et al. [22].

The computed NBO charges are reported in Table VI for the isolated complex **3** and with the presence of the Br atom, as it was experimentally reported, i.e., $[Au_2(\mu\text{-G})(\mu\text{-dmpe})]$ Br [22]. The electronic charge at the Au1 atom appears to be

TABLE VI
Selected NBO atomic charges of complex 3 and 3·Br.

Atom	$[Au_2(\mu\text{-G})(\mu\text{-dmpe})]$	$[Au_2(\mu\text{-G})(\mu\text{-dmpe})]Br$
Au1	0.536	0.535
Au2	0.551	0.561
P1	0.858	0.858
P2	0.866	0.855
N1	−0.875	−0.865
Br	—	−0.972

TABLE VII

Excitation energies, wavelengths (λ), and oscillator strengths (f) of complex 1.

	Energy (eV)	λ (nm)	f	Experimental energy (eV)
		CIS		
Triplet	2.02	614	0.0	2.22
Triplet	2.84	437	0.0	
Singlet	2.88	430	0.03	
Singlet	3.02	410	0.15	2.70
Triplet	3.06	405	0.0	
Singlet	3.34	371	0.06	
Triplet	3.38	367	0.0	

unchanged because no interaction is present with adjacent atoms. For the Au2 atom, a slight increment of charge is reported (about 0.01 electrons), indicating that the oxidation number +1 of the Au2 atom is basically unaltered. The 6s and 5d electronic population changes may be neglected. That is, the $6s^{0.86}$ population on compound [Au_2(μ-G)(μ-dmpe)] becomes $6s^{0.88}$ in the [Au_2(μ-G)(μ-dmpe)] Br complex, whereas the $5d^{9.67}$ population goes to $5d^{9.70}$. As a consequence, a change in the oxidation number from 1 to 2 is not observed. This is opposite to the results reported on analogous ring compounds [46], and an Au(I)-Au(II) bond is not formed. Nevertheless, the role of the Br atom is to polarize the Au2 atom, giving as a result the shortening of the Au—Au bonding. The Au2—Br long bonding distance (302 pm) corresponds to a weak interaction that keeps the +1 oxidation number unaltered.

3.3. EXCITED-STATE CALCULATIONS

To understand the absorption and emission bands of the series of complexes observed experimentally, excited-state calculations were performed at the CIS level from the MP2 ground-state geometry. The absorption band of compound **1** may be interpreted from the excited state corresponding to a singlet configuration, located at 410 nm (see Table VII). The oscillator strength for this excitation is 0.1522, indicating that this interaction corresponds to absorption. This result is in reasonable agreement with experimental data. For this excitation, the greatest CI coefficient is 0.4601, which may be addressed to the most likely transition taking place in the interaction. This coefficient corresponds to an excitation coming from the HOMO to the LUMO (HOMO → LUMO). The electronic density on the HOMO is mainly allocated on the i-mnt ligand. It is formed by π orbitals and a slight contribution coming from the Au d_{xz} orbitals (see Fig. 3).

When an electron excitation is activated, it is possible to determine the allocation that the electron will occupy from the spatial representation of the unoccupied MO. In this case, the electron will be excited to the LUMO at the central region on the ring and between the Au atoms. This indicates that the aurophilic attraction would be strengthened on the excited state.

The low-energy excited state at 614 nm may be interpreted as the phosphorescence seen in experiment and located at 558 nm. The greatest CI coefficient is 0.6341, which corresponds to a highly probable transition. In this situation, the decay of the electron goes from the LUMO, mainly composed of the Au 6s orbitals, to the HOMO, mainly formed by the π orbitals at the i-mnt ligand with a slight contribution from the Au d_{xz} orbitals, as it has been already stated. Taking the latter into account, this excitation corresponds

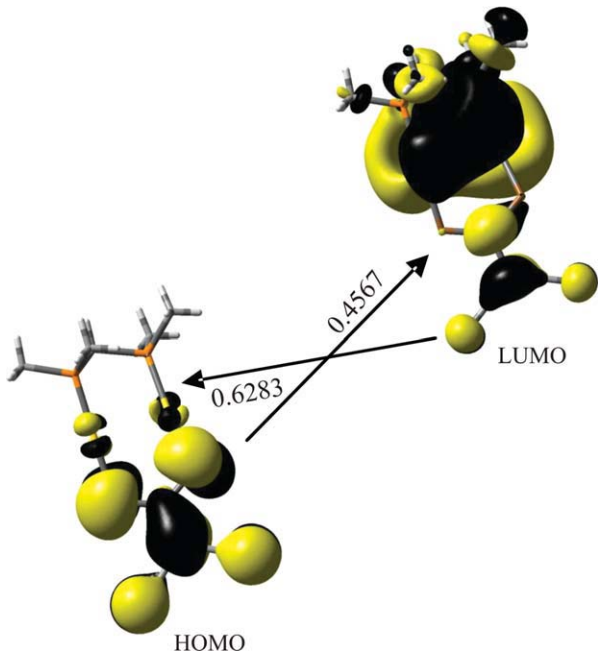

FIGURE 3. Frontier MOs involved in the transition with |CI coefficient| > 0.1 for the absorption and emission excitations for compound **1**. [Color figure can be viewed in the online issue, which is available at wileyonlinelibrary.com.]

TABLE VIII

Excitation energies, wavelengths (λ), and oscillator strengths (f) of complex 2.

	Energy (eV)	λ (nm)	f	Experimental energy (eV)
		CIS		
Triplet	2.41	514	0.0	2.56
Singlet	2.43	510	0.0011	
Triplet	2.61	475	0.0	
Triplet	2.95	420	0.0	
Singlet	3.11	398	0.0132	3.30

to a metal to ligand charge transfer (MLCT), with a small intraligand (IL) character (see Fig. 3).

The phosphorescent behavior observed by Lee and Eisenberg [16] on complex **2** was also studied according to the CIS method. The calculation was performed from the MP2 ground-state geometry. The results are presented in Table VIII. The experimental absorption band is located at 375 nm; the calculated excited state at 398 nm may be assigned to that transition. The largest CI coefficient is 0.7018, with a high probability that the excitation takes place. This is a transition coming from the HOMO to the LUMO + 1 (HOMO → LUMO + 1 transition). The HOMO is mainly allocated at the thiouracilate ligand and formed by the π orbitals from carbon and nitrogen (see Fig. 4). The HOMO has a slight contribution from the d_{xz} orbitals located at the Au atoms. LUMO + 1, a virtual orbital, provides information of the most likely region on the molecule where the electronic charge may be transferred. In this case, the electronic density is mainly located on the dppm ligand and it is formed by the C sp orbitals. The C atoms are those that bridge the P atoms at the upper region of the molecule (see Fig. 1); as a consequence, the interaction giving rise to the absorption band corresponds to an IL charge transfer.

The emission band found in the experiment is located at 483 nm; this transition may be assigned to the first excited state (see Table VIII), located at 514.0 nm with an excitation energy of 2.41 eV. The transition is a triplet that may be interpreted as the phosphorescence found by Lee and Eisenberg [16]. The highest CI coefficient corresponds to 0.6918; the interaction comes from the LUMO to the HOMO (LUMO → HOMO). The LUMO exhibits a mixture of sp orbitals allocated at the C atoms on the dppm ligand. As stated above, the HOMO is localized at the thiouracilate ligand,

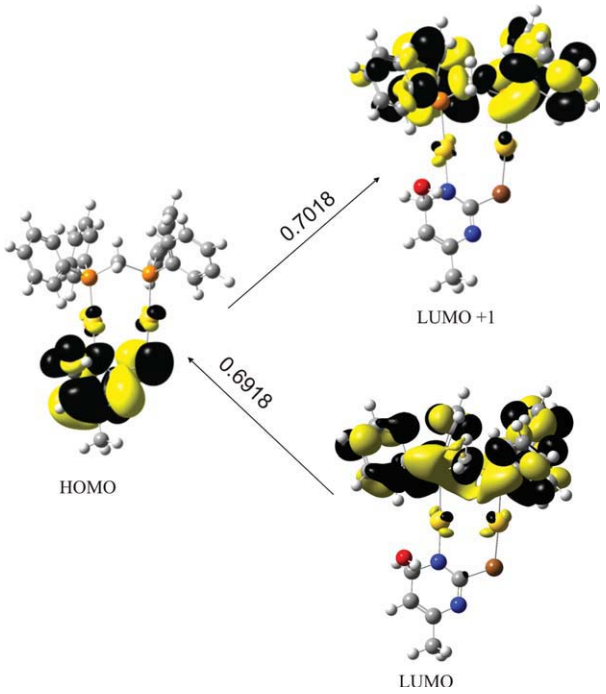

FIGURE 4. Frontier MOs involved in the transition with |CI coefficient| > 0.1 for the absorption and emission excitations for compound **2**. [Color figure can be viewed in the online issue, which is available at wileyonlinelibrary.com.]

mainly formed by π orbitals located at the N and C atoms. To explain the mechanism behind the transition originating the phosphorescence in complex **2**, the absorption process should be considered. An electron is excited from the HOMO to the virtual orbital LUMO + 1, where the electron subsequently resides. To produce the phosphorescence found in experiment, the singlet decays to a triplet. This interaction may be assigned to an intersystem crossing, where the electron undergoes a decay coming from the excited singlet configuration to the lower energy triplet. The electron decays to the ground-state configuration to stabilize the system (LUMO → HOMO transition), and an emission of light is produced during the process (see Fig. 4). According to the shape of the frontier MOs described above, the de-excitation giving rise to phosphorescence is produced by an IL transition.

As depicted in Figure 2, at the [Au_2(μ-MeTU)(μ-dppm)]$_2$ equilibrium geometry, the phenyl groups interact directly with the thiouracilate ligand, and the phosphorescence is generated by a charge transfer from the former to the latter. This may be related to the luminescence

tribochromism: The molecules in compound **2** would undergo a shrinkage on the intermolecular distances, strengthening the interaction among the thiouracilate and phenyl groups, giving as a consequence, the IL character and triggering the luminescence tribochromism phenomena.

With the aim of gaining an insight into the phosphorescent behavior observed experimentally on complex **3**, a CIS excited-state calculation was performed. The excited state located at 301 nm (4.12 eV) presents a nonzero oscillator strength that can be addressed to the absorption band located at 302 nm (see Table IX). The transition with the highest CI coefficient is depicted in Figure 5 and corresponds to an excitation coming from the HOMO to the LUMO + 1. According to the electronic population analysis, the charge at the HOMO is mainly located at the N and C atoms. The charge is transferred to the Au6sp orbitals at the LUMO + 1. As a consequence, it corresponds to an LMCT (ligand to metal charge transfer) interaction. The population analysis cannot be applied to unoccupied orbitals; nonetheless, it is possible to determine where the charge may be transferred, considering the shape of the isosurfaces, as depicted in Figure 5.

The excited state at 500 nm (see Table IX and Fig. 5) may be assigned to the emission observed experimentally and centered at 449 nm. The largest CI coefficient (0.114) represents an excitation coming from the LUMO, where the π orbitals, allocated at the guaninate, N, and C atoms, are involved in the interaction. Besides, a slight contribution from one of the Au d_{xz} orbitals is present. The charge is transferred to the HOMO, residing at the N and C atoms with Au d_{xz} contributions. Therefore, this transition may be assigned to an ILMCT, mixed with a metal to metal centered charge transfer interaction.

TABLE IX

Excitation energies, wavelengths (λ), and oscillator strengths (f) of complex 3.

	Energy (eV)	λ (nm)	f	Experimental energy (eV)
		CIS		
Triplet	2.48	500	0.0	2.76
Singlet	2.64	470	0.0214	
Singlet	2.76	449.53	0.2301	
Triplet	3.70	335.3	0.0	
Singlet	4.12	301	0.0280	4.10

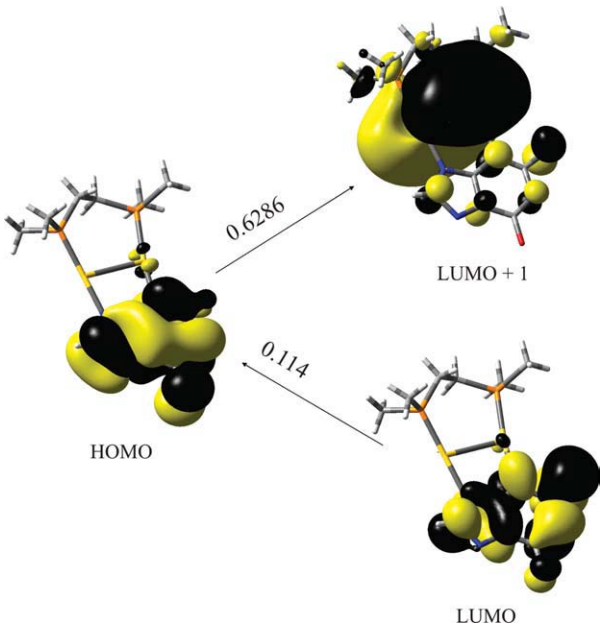

FIGURE 5. Frontier MOs involved in the transition with |CI coefficient| > 0.1 for the absorption and emission excitations for compound **3**. [Color figure can be viewed in the online issue, which is available at wileyonlinelibrary.com.]

4. Conclusions

An ab initio study was carried out on a series of dinuclear Au(I) compounds. The intramolecular and intermolecular aurophilic attractions experimentally observed in the series may be attributed to dispersive effects, strengthened by the breaking of the Au(I) closed-shell structure. The computed intermolecular bonding energy in complexes **2** and **3** is on the aurophilic range. The electronic charge excess in the frontier MOs, allocated at the intermediate region, also contributes to the interaction. One of the mechanisms present in the phosphorescent behavior of the series of complexes may be assigned to the strengthening of the aurophilic attraction in the excited state. Therefore, MLCT and IL transitions are found on the systems under study. Thus, it was observed that the IL behavior in complex **2** depends on the electronic transfer from the phenyl groups to the thioracilate. These excitations may be produced on an intermolecular interaction bridged by the ligands. The intermolecular attraction appears to be a necessary condition for the rising of the phosphorescence in this kind of systems.

ACKNOWLEDGMENTS

The computing time provided by DGSCA–UNAM and CNS-IPICyT is acknowledged.

References

1. Vickery, J. C.; Olmstead, M. M.; Fung, E. Y.; Balch, A. L. Angew Chem Int Ed Engl 1997, 36, 1179.
2. Chan, W. H.; Mak, T. C. W.; Che, C. M. J Chem Soc Dalton Trans 1998, 14, 2275.
3. Mansour, M. A.; Connick, W. B.; Lachicotte, R. J.; Gysling, H. J.; Eisenberg, R. J Am Chem Soc 1998, 120, 1329.
4. Blonder, R.; Levi, S.; Tao, G.; Ben-Dov, I.; Willner, I. J Am Chem Soc 1997, 119, 10467.
5. Wolf, M. O.; Fox, M. A. J Am Chem Soc 1995, 117, 1845.
6. Lu, X.; Yavuz, M. S.; Tuan, H.-Y.; Korgel, B. A.; Xia, Y. J Am Chem Soc 2008, 130, 8900.
7. Quiroga, A. G.; Pérez, J. M.; López-Solera, I.; Masaguer, J. R.; Luque, A.; Román, P.; Edwards, A.; Alonso, C.; Navarro-Ranninger, C. J Med Chem 1998, 41, 1399.
8. Sadler, P. J. Adv Inorg Chem 1991, 36, 1.
9. Mirabelli, C. K.; Jonson, R. K.; Hill, D. T.; Faucette, L. F.; Girard, G. R.; Kuo, G. Y.; Sung, C. M.; Crooke, S. T. J Med Chem 1986, 29, 218.
10. Corey, E. J.; Mahrota, M. M.; Khan, A. U. Science 1987, 236, 68.
11. Mohamed, A. A.; Galassi, R.; Papa, F.; Burini, A.; Fackler, J. P., Jr. Inorg Chem 2006, 45, 7770.
12. van Zyl, W. E.; López-de-Luzuriaga, J. M.; Fackler, J. P., Jr. J Mol Struct 2000, 516, 99.
13. Parks, J. E.; Balch, A. L. J Organomet Chem 1974, 71, 453.
14. Balch, A. L.; Doonan, D. J. J Organomet Chem 1997, 131, 137.
15. Mansour, M. A.; Connick, W. B.; Lachicotte, R. J.; Gysling, H. J.; Eisenberg, R. J Am Chem Soc 1998, 120, 1329.
16. Lee, Y.-A.; Eisenberg, R. J Am Chem Soc 2003, 125, 7778.
17. Muñiz, J.; Sansores, L. E.; Martínez, A.; Salcedo, R. J Mol Struct (THEOCHEM) 2007, 820, 141.
18. Muñiz, J.; Wang, C.; Pyykkö, P. Chem Eur J 2010 (in press).
19. Pyykkö, P. Chem Rev 1997, 97, 597.
20. Pyykkö, P. Angew Chem Int Ed 2004, 43, 4412.
21. Tang, S. S.; Chang, C.-P.; Lin, I. J. B.; Liou, L.-S.; Wang, J.-C. Inorg Chem 1997, 36, 2294.
22. Colacio, E.; Crespo, O.; Cuesta, R.; Kivekäs, R.; Laguna, A. J Inorg Biochem 2004, 98, 595.
23. Pan, Q.-J.; Zhang, H.-X. J Chem Phys 2003, 119, 4346.
24. Pan, Q.-J.; Zhang, H.-X. Eur J Inorg Chem 2003, 23, 4202.
25. Muñiz, J.; Sansores, L. E.; Martínez, A.; Salcedo, R. J Mol Struct (THEOCHEM) 2009, 901, 232.
26. Møller, C.; Plesset, M. S. Phys Rev 1934, 46, 618.
27. van Lenthe, E.; Snijders, J. G.; Baerends, E. J. J Chem Phys 1996, 105, 6505.
28. Fang, H.; Wang, S.-G. J Phys Chem A 2007, 111, 1562.
29. Andrae, D.; Haeussermann, U.; Dolg, M.; Stoll, H.; Preuss, H. Theor Chim Acta 1990, 77, 123.
30. ftp://ftp.chemie.uni-karlsruhe.de/pub/basen.
31. Schäfer, A.; Huber, C.; Ahlrichs, R. J Chem Phys 1994, 100, 5829.
32. Pyykkö, P.; Runeberg, N.; Mendizabal, F. Chem Eur J 1997, 3, 1451.
33. Schäfer, A.; Horn, H.; Ahlrichs, R. J Chem Phys 1992, 97, 257.
34. Boys, S. F.; Bernardi, F. Mol Phys 1970, 19, 553.
35. Klopper, W.; Kutzelnigg, W. Chem Phys Lett 1987, 134, 17.
36. Klopper, W. Chem Phys Lett 1991, 186, 583.
37. Klopper, W.; Samson, C. C. M. J Chem Phys 2002, 116, 6397.
38. Manby, F. R. J Chem Phys 2003, 119, 4607.
39. Foresman, J. B.; Head-Gordon, M.; Pople, J. A.; Frisch, M. J. J Phys Chem 1992, 96, 135.
40. Weinhold, F. In: Natural Bond Orbital Methods; Encyclopedia of Computational Chemistry; Schleyer, P. v. R.; Allinger, N. L.; Clark, T.; Gasteiger, J.; Kollman, P. A.; Schaefer III, H. G.; Schreiner, P. R., Eds.; John Wiley & Sons: Chichester, UK, 1998; Vol 3, p 1792.
41. Ahlrichs, R.; Bär, M.; Häser, M.; Horn, H.; Kölmel, C. Chem Phys Lett 1989, 162, 165.
42. Ahlrichs, R.; von Arnim, M. In Methods and Techniques in Computational Chemistry: METECC-95; Clementi, E., Corongiu, G., Eds.; STEP: Cagliari, 1995;Chapter 13, p 509.
43. Frisch, M. J.; Trucks, G. W.; Schlegel, H. B.; Scuseria, G. E.; Robb, M. A.; Cheeseman, J. R.; Montgomery, J. A., Jr.; Vreven, T.; Kudin, K. N.; Burant, J. C.; Millam, J. M.; Iyengar, S. S.; Tomasi, J.; Barone, V.; Mennucci, B.; Cossi, M.; Scalmani, G.; Rega, N.; Petersson, G. A.; Nakatsuji, H.; Hada, M.; Ehara, M.; Toyota, K.; Fukuda, R.; Hasegawa, J.; Ishida, M.; Nakajima, T.; Honda, Y.; Kitao, O.; Nakai, H.; Klene, M.; Li, X.; Knox, J. E.; Hratchian, H. P.; Cross, J. B.; Bakken, V.; Adamo, C.; Jaramillo, J.; Gomperts, R.; Stratmann, R. E.; Yazyev, O.; Austin, A. J.; Cammi, R.; Pomelli, C.; Ochterski, J. W.; Ayala, P. Y.; Morokuma, K.; Voth, G. A.; Salvador, P.; Dannenberg, J. J.; Zakrzewski, V. G.; Dapprich, S.; Daniels, A. D.; Strain, M. C.; Farkas, O.; Malick, D. K.; Rabuck, A. D.; Raghavachari, K.; Foresman, J. B.; Ortiz, J. V.; Cui, Q.; Baboul, A. G.; Clifford, S.; Cioslowski, J.; Stefanov, B. B.; Liu, G.; Liashenko, A.; Piskorz, P.; Komaromi, I.; Martin, R. L.; Fox, D. J.; Keith, T.; Al-Laham, M. A.; Peng, C. Y.; Nanayakkara, A.; Challacombe, M.; Gill, P. M. W.; Johnson, B.; Chen, W.; Wong, M. W.; Gonzalez, C.; Pople, J. A. Gaussian 03, Revision E.01; Gaussian, Inc.: Wallingford, CT,2004.
44. Wiberg, K. B. Tetrahedron 1968, 24, 1083.
45. Muñiz, J.; Sansores, L. E.; Martínez, A.; Salcedo, R. J Mol Model 2008, 14, 417.
46. Pyykkö, P.; Mendizabal, F. Inorg Chem 1998, 37, 3018.